Functional CT: physiological models

Ting-Yim Lee

Since its introduction three decades ago, computed tomography (CT) has been regarded as an imaging technique that is good at providing structural information but poor at providing physiological (functional) data to help with diagnosis. For instance, although it can reveal an abnormal mass present in the lung or liver, it cannot always differentiate a benign mass from a malignant growth. The introduction of fast CT scanners in the past decade, together with the development of better analysis techniques, has helped to launch functional CT as a new method to investigate the physiological basis of function and disease in the human body.

Ladurner and colleagues [1] were the first to use computed tomography (CT) to study physiological function in the human brain by measuring cerebral blood volume with intravenously injected X-ray contrast agent (an iodinated compound that preferentially stops X-rays more effectively than tissue). They used an equilibrium technique in which CT scanning was done at a time when the injected contrast agent had established an equilibrium distribution throughout the whole body. An alternative technique, called dynamic CT, uses serial CT scans at the same location to study the distribution of contrast agent in the brain as a function of time, and was first used by Traupe *et al.* [2].

From these early beginnings, dynamic CT methodology has evolved through several generations of technological advances in CT technology [3], and dynamic CT has become the dominant CT method in the evaluation of (physiological) function within the human body. The technique has thus been termed functional CT. The important advantages of functional CT in comparison to other imaging modalities, such as magnetic resonance imaging or positron emission tomography, are its accessibility and simplicity. Functional CT makes use of conventional CT scanners in radiology departments so it is available to patients 24 hours per day. In addition, the method only involves the intravenous injection of conventional contrast agent and CT scanning, enabling the study to be easily performed without extensive additional training of staff.

Basis of functional CT

The intensity of a CT image, expressed as Hounsfield units [4], is related to the efficiency with which X-rays are stopped (attenuated) as they traverse the volume element (voxel) in the human body, and are represented by the picture element (pixel) in the CT image. The basis of functional CT is to inject contrast agent intravenously and then measure the increase in attenuation or enhancement of the tissue after arrival of the contrast agent by CT scanning or contrast-enhanced CT scanning. Thus, the very first data processing step of functional CT is to subtract the baseline image intensity from the image intensity after the arrival of contrast. One important advantage of CT is that the enhancement is linearly proportional to the concentration of contrast agent in the tissue.

With the equilibrium technique, two scans – one baseline, and another at a time when the contrast agent has equilibrated throughout the whole body – permit the calculation of the equilibrium enhancement by simple subtraction. With contrast-enhanced dynamic CT, serial CT scans start before the contrast agent arrives (to determine the baseline) and continue until the contrast agent leaves the tissues. Subtraction of the baseline from each of the serial CT scans after the arrival of the contrast agent at the tissue gives the time-versus-enhancement or time-density curve (TDC) of the tissue. All the physiological (functional) information about a tissue is obtained by mathematical or tracer kinetic analysis of the tissue TDC. These analyses are based on proposed 'tracer kinetics' models that describe the distribution of contrast in blood vessels and extravascular space of the tissue [5].

Technical requirements

For the equilibrium methodology, the speed of CT scanning does not need to be very high because the baseline scan can be performed at any time before injection of contrast agent, and the equilibrium scan at any time after the contrast agent has equilibrated with the whole body. For example, Ladurner and colleagues [1] successfully measured cerebral blood volume at a scanning speed of 10 s per scan. The minimum transit time of a tissue, defined as the time from arrival of a tight bolus of the contrast agent at the tissue to the first exit of the contrast agent from the tissue, is generally 4–10 s.

For dynamic CT, if the tissue TDC is to be measured with adequate detail, the speed of each scan has to be of the order of <1 s. This speed requirement has been addressed with the advent of slip-ring CT scanners [3]. Before the introduction of the slip-ring design, the high tension (voltage) required to generate X-rays was applied

Ting-Yim Lee
Imaging Research Laboratories, Robarts Research Institute and Lawson Health Research Institute, 100 Perth Drive, London, Ontario, Canada N6A 5K8.
e-mail: tlee@irus.rri.ca

0167-7799/02/$ – see front matter PII: S0167-7799(02)02027-9

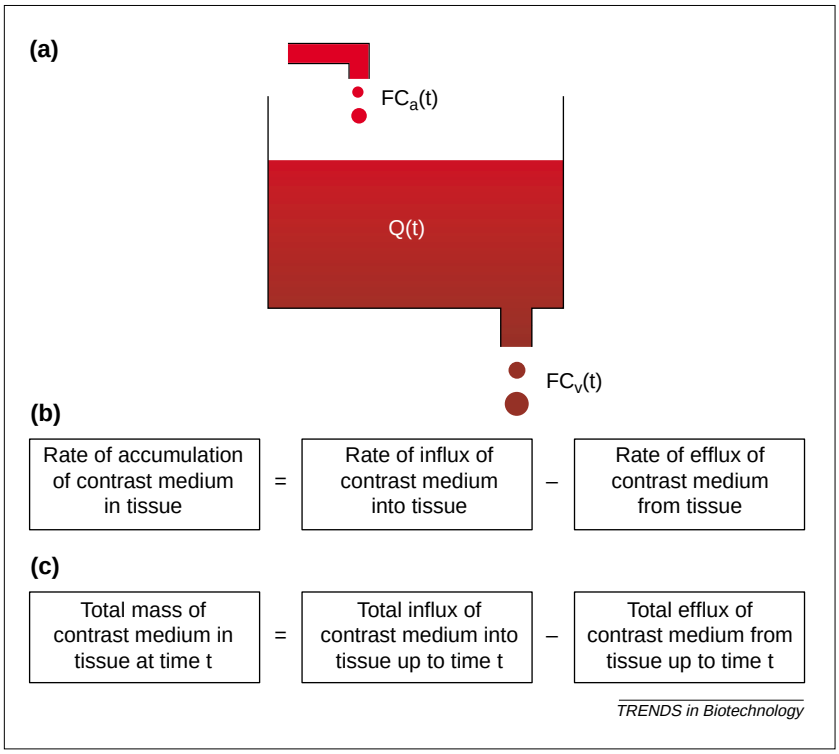

Figure 1. The Fick Principle

(a) Schematic representation of the Fick Principle. F is blood flow to a tissue, $C_a(t)$ is the arterial concentration of contrast agent, $C_v(t)$ is the venous concentration of contrast agent and Q(t) is the mass of contrast agent in the brain at any time. (b) The differential form of the Fick Principle. (c) The integral form of the Fick Principle.

to the X-ray tube in the CT scanner gantry via cables from a high-tension transformer outside of the gantry. As a result, the X-ray tube cannot rotate in one direction continuously because after one revolution in one direction the cables have to be unwound by rotation in the opposite direction. By contrast, the slip-ring design supplies the high tension to the X-ray tube via metallic brushes that continuously make contact with a metal ring in the gantry – hence the name slip-ring. By eliminating the high-tension cables, the X-ray tube is able to rotate continuously around the subject at a speed of 0.5–1.0 s per rotation.

Tracer kinetic analysis

The different tracer kinetics models can be grouped as follows: model-independent approaches for blood flow measurements based on the Fick Principle and deconvolution analysis; compartmental modeling as exemplified by the Patlak model [6]; and modeling that accounts for convective transport (blood flow) and diffusional exchange (capillary permeability) via a distributed parameter model as proposed by Johnson and Wilson [7].

Model independent approaches

Fick Principle. The Fick Principle is applied to an inert material (e.g. contrast agent) that is not sequestered or metabolized by the tissue (see Fig. 1). Figure 1a lends itself to two interpretations as shown in Figs 1b and c.

In mathematical terms, the first interpretation (Fig. 1b) can be expressed as:

$$\frac{dQ(t)}{dt} = FC_a(t) - FC_v(t) \qquad \text{[Eqn 1a]}$$

Where F is blood flow to the tissue, $C_a(t)$ is the arterial concentration of contrast agent, $C_v(t)$ is the venous concentration of contrast agent, and Q(t) is the mass of contrast agent in the brain at any time.

The second interpretation (Fig. 1c) is:

$$Q(t) = F\int_0^t C_a(t)dt - F\int_0^t C_v(t)dt \qquad \text{[Eqn 1b]}$$

In contrast-enhanced dynamic computed tomography, Q(t) is the TDC measured in the tissue, and $C_a(t)$ is the TDC measured in an arterial region in the tissue.

No venous outflow assumption. At times less than the minimum transit time, all of the injected contrast medium will remain within the tissue. Under this assumption, Eqn 1a simplifies to:

$$\frac{dQ(t)}{dt} = FC_a(t)$$

which can be rearranged to estimate blood flow as:

$$F\frac{\frac{dQ(t)}{dt}}{C_a(t)} \qquad \text{[Eqn 2]}$$

or equivalently as:

$$F = \frac{\text{Maximum initial slope of } Q(t)}{\text{Peak height of } C_a(t)}$$

Thus, under the assumption of no venous outflow, tissue blood flow can be simply calculated as the ratio of the maximum initial slope of the tissue TDC to the peak height of the arterial TDC. This method was proposed by Peters *et al.* [8], and later used by Miles [9] in the CT measurement of tissue perfusion in a variety of abdominal organs. More recently, the method was used by Klotz *et al.* to determine cerebral blood flow (CBF) [10].

The main advantage of this method is its conceptual simplicity. However, a major disadvantage is that, in general, the assumption of no venous outflow at the time of the maximum initial slope of the tissue TDC is not always true. If there is significant venous outflow of contrast medium before the maximum initial slope of the tissue TDC is reached, then underestimation of blood flow will occur. In addition, when the artery used to the generate the arterial TDC is small in comparison to the spatial resolving power of the CT scanner, averaging the arterial signal with the surrounding tissue signal, or volume averaging will lead to an underestimation of the peak height of the arterial TDC, and hence an overestimation of blood flow [11]. It is worth noting that the volume-averaging effect on the arterial TDC affects all tracer kinetics analysis methods, not just the Fick Principle-based method.

Draining vein assumption. If a 'local' draining vein can be identified, then Eqn 1b can be used to calculated blood flow as follows [12]:

$$F = \frac{Q(t)}{\int_0^t C_a(t)dt - \int_0^t C_v(t)dt} \qquad \text{[Eqn 3]}$$

For this method to apply, it is implicitly assumed that all TDCs – arterial, tissue and venous – are properly aligned in time; that is, there are no time delays among the three TDCs. Misalignments of the TDCs will also lead to errors in blood-flow calculations.

Again, the main advantage of this method is conceptual simplicity. The main disadvantage is that the technique cannot be used to generate blood flows of individual voxels of a tissue (i.e. blood flow maps) because the venous outflow cannot be measured for individual voxels. In addition, as is usually the case, the identified draining vein is small in comparison to the spatial resolving power of the CT scanner, meaning that volume averaging would lead to underestimation of the venous AUC (area underneath the curve) and, consequently, underestimation of the blood flow. Similarly, volume averaging of arterial TDC would result in the overestimation of blood flow.

Method of moments. This class of method only applies when there is no leakage of contrast agent from the blood stream into the extravascular space, for example, in the brain when the blood–brain barrier is intact. Axel showed that cerebral blood volume (CBV) can be calculated according to the formula [13]:

$$CBV = \frac{\text{AUC of extrapolated tissue TDC}}{\text{AUC of extrapolated arterial TDC}}$$

Extrapolation of both arterial and tissue TDCs removes the effect of recirculation of the contrast agent. As blood (and therefore contrast agent) traverses the tissue vasculature through different pathlengths, there is no unique transit time from the arterial inlet to the venous outlet. Instead, there is a distribution of transit times, and MTT (mean transit time) is the mean time of such a distribution [14]. MTT has been shown to be inversely correlated to the perfusion pressure [15]. In the determination of CBF, Gobbel *et al.* showed that the difference in the center of gravity of the AUCs of extrapolated tissue- and arterial-TDCs can be expressed in terms of the MTT and the spread of the transit times about the MTT as characterized by the variance of the transit times [16]:

$$\boxed{\text{Center of gravity of the AUC of the extrapolated tissue TDC}} - \boxed{\text{Center of gravity of the AUC of the extrapolated arterial TDC}} = \frac{1}{2}\text{MTT} + \frac{1}{2}\frac{\sigma^2}{\text{MTT}}$$

where σ is the variance of the transit times.

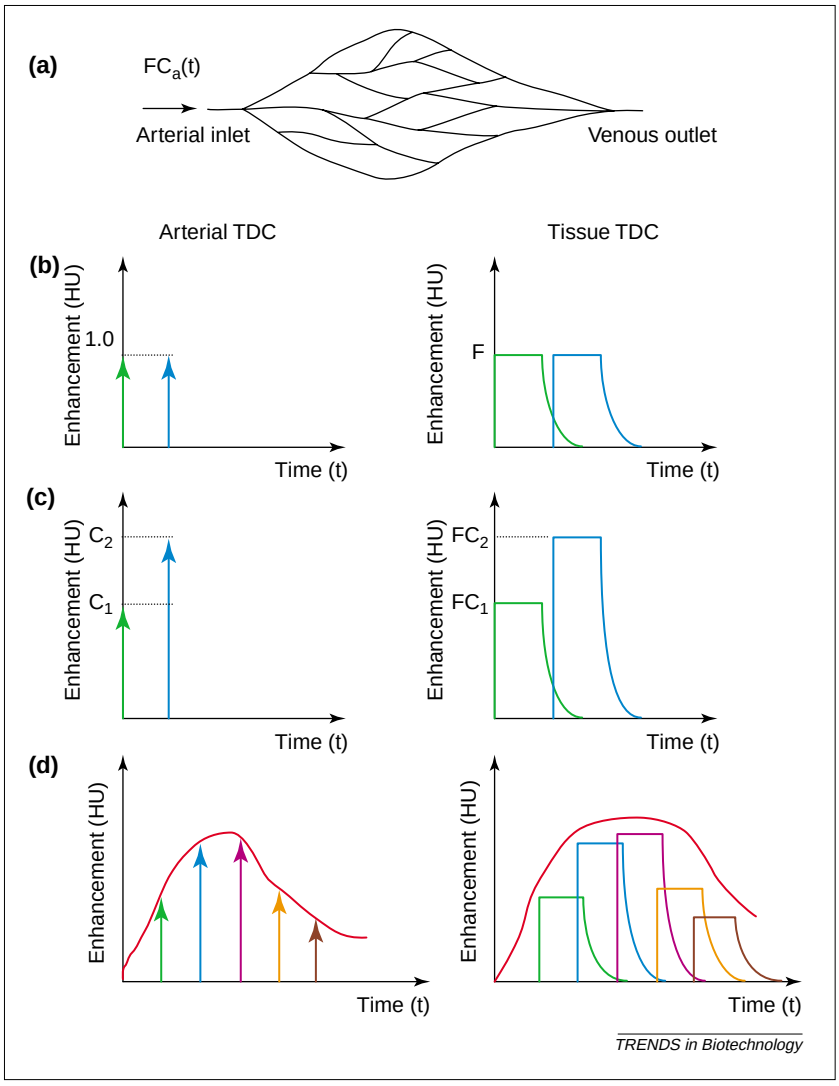

Figure 2. The concept of convolution

(a) Schematic representation of the vasculature of a tissue region. The rate of input of contrast agent into the tissue is $FC_a(t)$. (b) If blood flow is unchanged (i.e. stationary) between two identical bolus injections of the same concentration (left panel), then the tissue time density curve (TDC) corresponding to each injection will be the same; this is termed the impulse residue function (IRF) of the tissue [17]. The IRF is a theoretical concept and cannot easily be measured in clinical practice. The right panel shows two IRFs corresponding to the case of two identical bolus injections of contrast agent of the same concentration. For each IRF, initially, there is an abrupt rise in the shape of the graph because the injection is directly into the arterial input, it then plateaus for a duration equal to the minimum transit time through the tissue region, and finally decays towards the baseline. (c) Tissue TDC corresponding to another special case when the arterial TDC consists of two bolus injections of different concentrations C_1 and C_2; the tissue TDC corresponding to this case is shown in the right panel. (d) Finally, a general arterial TDC can be represented as a series of bolus injections equally spaced in time and of different concentrations (left panel). For each bolus injection, tissue TDC is a scaled IRF, which is the product of blood flow, concentration of bolus, and the IRF. The total tissue TDC in response to the general arterial concentration $C_a(t)$ is the sum of all the scaled IRFs after they have been shifted in time in accordance to the times of their corresponding bolus injection. Abbreviation: HU, Hounsfield units.

This equation can be rearranged to:

$$\text{MTT} = \frac{2 \times \text{Difference in center of gravity between tissue and arterial TDC}}{1 + k^2}$$

where k is the ratio of σ to MTT. Thus, provided k is known, MTT can be calculated using this equation, and CBF can be calculated as the ratio of CBV to MTT, according to the

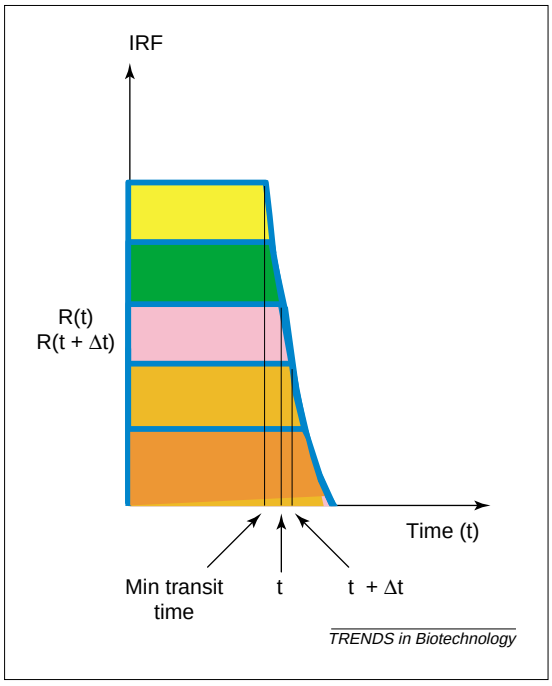

Figure 3. Mean transit time is the area under the curve

The impulse residue function (IRF) can be viewed as the fraction of contrast medium that remains in the tissue as time evolves, following a bolus injection into the arterial input. Beyond the minimum transit time (the duration of the plateau), the difference of R(t + Δt) and R(t) is the fraction of contrast medium that has a transit time of t. This difference is the height of the strip with a transit time of t. Furthermore, the area of each of the horizontal strips is the product of the transit time and the fraction of contrast medium having that transit time. It then follows that the area of all the horizontal strips in the figure, that is, the area under the curve (AUC) of R(t), is the mean transit time (MTT). Alternatively, as the Central Volume Principle [14] states that the product of F and MTT is blood volume, the AUC of FR(t) is the blood volume.

Central Volume Principle [14]. Gobbel *et al.* assumed that k is relatively uniform throughout the brain and estimated it with a pair of arterial and venous TDCs measured in an extracranial artery and an intracranial vein, respectively [16].

The advantage of this method is that it does not require the assumption of no venous outflow. However, the assumption that k remains relatively uniform throughout the brain, in general, might not be true, particularly for ischemic tissue.

Deconvolution-based methods

This class of method is dependent on the concept of convolution (see Fig. 2). In general, if the impulse residue function (IRF) is known, the tissue TDC in response to a general arterial TDC, $C_a(t)$, can be obtained as a summation of scaled and time-shifted IRFs. The scale factors and time shifts are given by $FC_a(t)$ and t, respectively. This operation is called a convolution (see Fig. 2d). Thus,

$$Q(t) = FC_a(t) \otimes R(t) = C_a(t) \otimes FR(t) \qquad \text{[Eqn 4]}$$

where ⊗ is the convolution operator, Q(t) is the tissue TDC, and FR(t) is the blood-flow scaled IRF.

By contrast, the derivation in contrast-enhanced dynamic CT is the reverse of the above discussion. Here, the arterial and tissue TDC are measured, but the problem becomes the calculation of FR(t), given Q(t) and $C_a(t)$, or deconvolution. Whereas convolution gives a unique (unambiguous) answer because it is a summation operation of the known IRF, deconvolution requires an estimation of the unknown FR(t) such that its convolution with the arterial TDC would approximate the tissue TDC. It is clear that deconvolution cannot give a unique answer because there would certainly be more than one FR(t) that would, after convolution with $C_a(t)$, give an equally good or better approximation to the tissue TDC. To complicate matters further, some of those 'equivalent' FR(t)s would have shapes that are completely different from that shown in Fig. 2b. This unstable characteristic of the deconvolution operation is caused by noise effects either in the arterial- or tissue-TDC [18]. However, with effective noise suppression, the FR(t) obtained by deconvolution can be further processed to calculate blood flow and other information [11]. The plateau height of FR(t) is the blood flow, F, and Fig. 3 explains how blood volume can be calculated from FR(t).

Compartmental modelling

Following injection into the blood stream, contrast agent will pass into the extravascular space of most tissues (excluding normal brain) at a rate that is characterized by a rate constant K. There is also exchange from the extravascular into the intravascular space with a rate constant K/V_e, where V_e is the extravascular distribution space of contrast. The theoretical basis of imaging K is the Patlak graphical analysis [6], which assumes that the injected contrast agent is distributed in two well-mixed compartments: the intravascular (blood) compartment and the extravascular compartment.

At any given time, a voxel of tissue will contain both intravascular and extravascular contrast agent. Assuming that during the time interval 0–t there is negligible backflux (return) of contrast agent from the extravascular to blood space, the total concentration of contrast agent in the tissue at time t, can be expressed as:

$$Q(t) = V_b C_a(t) + K\int_0^t C_a(u)du \qquad \text{[Eqn 5]}$$

where V_b is the blood volume of the tissue. In Eqn 5, the first term on the right side expresses the intravascular component of enhancement and the second term describes the extravascular component.

The Patlak graphical analysis divides both sides of Eqn 5 by $C_a(t)$ to give:

$$\frac{Q(t)}{C_a(t)} = V_b + K\frac{\int_0^t C_a(u)du}{C_a(t)} \qquad \text{[Eqn 5a]}$$

and plots

$$\frac{Q(t)}{C_a(t)}$$

on the y-axis and

$$\frac{\int_0^t C_a(u)du}{C_a(t)}$$

on the x-axis, yielding a straight line with slope K and intercept V_b [19,20].

To avoid making the assumption that the back-flux of contrast from the extravascular space to the intravascular space is negligible, several investigators [21–25] implemented the full solution of the Patlak two-compartmental model to obtain:

$$Q(t) = V_b C_a(t) + K\int_0^t C_a(u) e^{-\frac{K}{V_e}(t-u)} du \quad \text{[Eqn 6]}$$

and used non-linear regression techniques to derive K and V_b in brain tumors and liver.

Compared with the non-linear regression method given in Eqn 6, the advantage of the Patlak graphical analysis given in Eqn 5a is its simplicity and, hence, efficiency in the calculation of functional maps of K and V_b. However, the assumption that back-flux from extravascular into intravascular can be neglected during early times will depend on the relative magnitude of blood flow and the capillary permeability surface area product (PS) [26]. Permeability (P) is related to the diffusion coefficient of contrast agent in the assumed water-filled pores of the capillary endothelium. The diffusion flux of contrast agent across the capillary endothelium is dependent on both the diffusion coefficient and the total surface area of the pores or the PS product. The relative magnitude of PS and F also determines the extraction fraction (E) of the contrast agent according to the relationship [27]:

$$E = 1 - e^{-\frac{PS}{F}}$$

More specifically, E is the fraction of the mass of contrast agent arriving at the tissue that leaks into the extravascular space in a single passage through the vasculature.

There are three regimes for the distribution of contrast agent between blood and extravascular space [28]: (i) when PS<<F, K approximates PS; (ii) when PS = F, K is equal to the product of FE so that separate determination of F and E is not possible; and (iii) when PS>>F (so that E approaches 1), K = F. However, even in the third regime, the finite transit time of contrast through the capillaries would lead to an inaccurate determination of blood flow when compartment models are used [29], and, more importantly, the arterial concentration will be higher than the venous concentration, meaning the intravascular space can no longer be regarded as a compartment.

Distributed parameter models

A general model that applies to all values of PS relative to F was first proposed by Johnson and Wilson [7]. It incorporates a concentration gradient within the intravascular space (capillary) from the arterial inlet to the venous outlet, modelling the extravascular space as a compartment. The complexity of the original solution, being in the Laplace domain, has hindered its acceptance into general usage since its first derivation. St Lawrence and Lee [28] discovered a simple analytical solution of the model in the time domain that is computationally efficient. Similar to the deconvolution method, the advantage of this simplified solution of the Johnson and Wilson model is that it enables the simultaneous determination of four physiological parameters: blood flow, blood volume, mean transit time and capillary permeability, from a single CT study [30,31]. In this respect, both methods are extremely versatile in situations where one would expect a wide range of PS values relative to F (e.g. in tumors).

The input or reference artery

As discussed previously, the input arterial concentration $C_a(t)$ is required to derive the functional parameters independent of the tracer kinetics model used. For example, if the aorta or other large branches of the aorta (e.g. femoral arteries) are visible within the CT images, then these vessels could serve as the input (reference) artery. In the brain, arterial concentration can be measured within arteries, provided a correction for partial volume averaging is applied [11]. This correction is necessary because the size of arteries in the brain are too small for the CT scanner to resolve accurately; as a result, any concentration measurement within a brain artery will be contaminated by contributions from the surrounding tissue. When stroke affects part of the brain, arteries in that part cannot be used as the input artery for normal brain because arterial concentration measured here will include the effect of collateral circulation, which is not present in the normal brain. In ischemic (low in blood flow) parts of the brain, the question of whether the input artery should be the affected arteries or the unaffected arteries on the contra-lateral 'normal' side, remains open at the present time. Further research will be required to resolve this issue.

Validation and reproducibility

The accuracy and precision of measured parameters are important considerations in the application of functional CT. In the measurement of blood flow, Cenic *et al.* [11] and Purdie *et al.* [30] validated their blood flow measurements against the *ex vivo* 'gold standard' of microspheres (which are independent of any tracer kinetics modeling). Furthermore, Nabavi *et al.* [32] showed that brain infarct size determined by their CBF measurement correlated well with that obtained with 2,3,5-triphenyltetrazolium chloride (TTC)-staining in a stroke model. Preliminary results from Lee *et al.* suggest that the precision of CBF measurements in normal subjects is around 14%. To advance the

Figure 4. Examples of application of functional CT

(a),(b) Mismatch of cerebral blood flow and cerebral blood volume (white arrows) in a stroke patient. (c),(d) Increased blood flow and capillary permeability surface area (PS) product (white arrows) in a prostate tumor. (e),(f) The blood flow map in two long-axis slices of the myocardium of a normal beagle. The low blood flow in the apical region of the myocardium (white arrows) are artifacts owing to beam hardening from contrast agent present in the left ventricle [40].

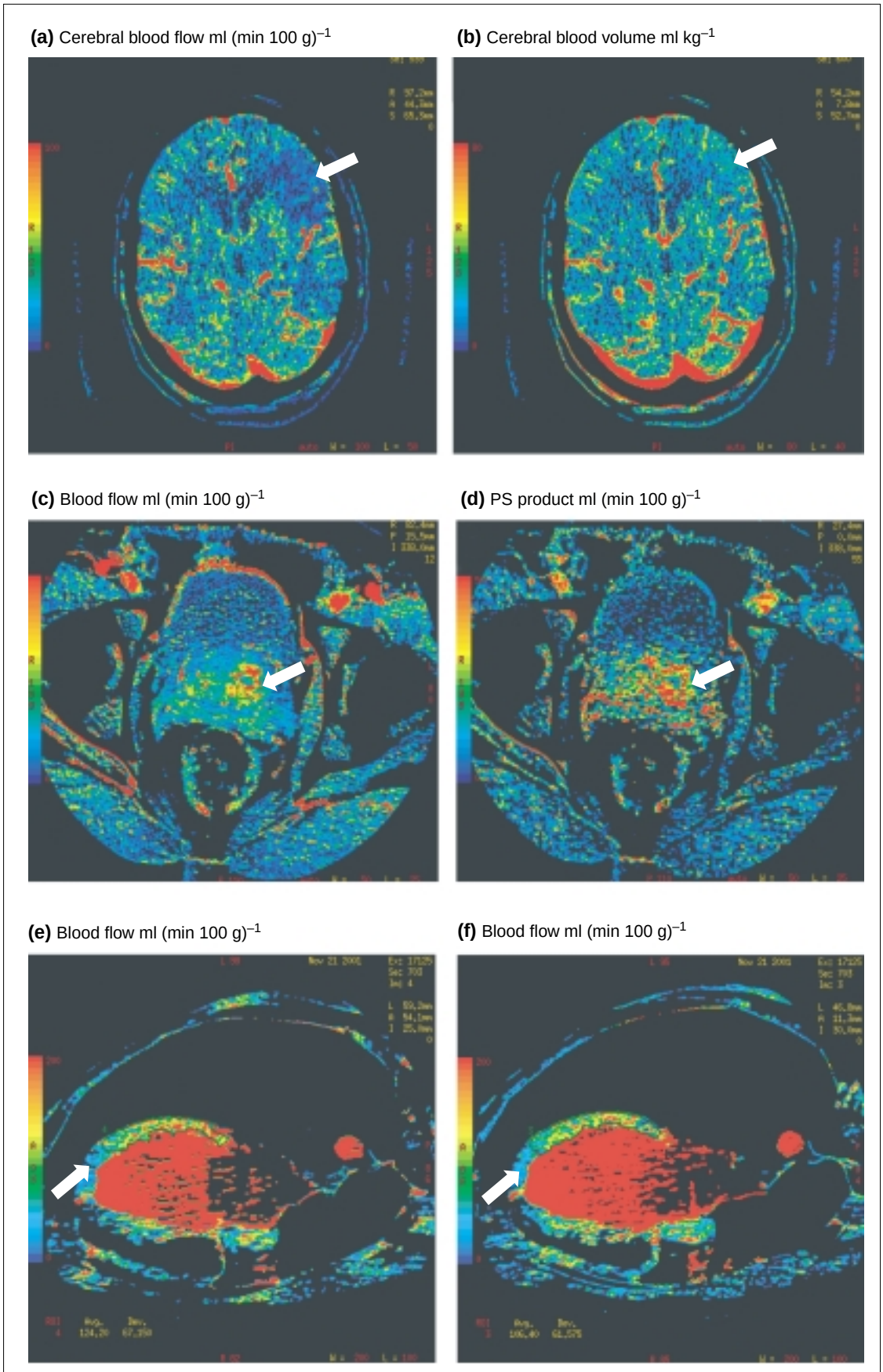

use of functional CT, further studies on the accuracy and precision of measured parameters other than blood flow must be conducted.

Applications

Functional CT has been applied to study stroke and cancer. The application to ischemic heart disease is currently under active development.

Stroke

Although stroke is the third leading cause of death, it is the number one cause of disability among adults in the western world. The degree of recovery following stroke is closely related to the extent of viable brain tissue present in the ischemic zone. Several groups of investigators have successfully implemented either contrast-enhanced dynamic CT to measure CBF, volume and mean transit time simultaneously [33–35], or equilibrium CT to measure cerebral blood volume [36,37]. A very interesting finding by Wintermark *et al.* [35] is that if an ischemic region has high or normal blood volume, or a flow and volume mismatch, then the tissue is viable. If blood flow to viable tissue is restored early, the tissue can recover its normal function. Figures 4a and b demonstrate the flow and volume mismatch in a patient following acute stroke when the measurement was performed 3 h after symptom onset. The blood flow and blood volume maps were calculated using the same method as Eastwood *et al.* [34].

Cancer

Miles *et al.* [38] recently reviewed the application of functional CT to the detection of angiogenesis associated with malignant tumors. As angiogenesis promotes the proliferation of endothelial cells that sprout structurally malformed vessels, CT contrast-enhancement was shown to correlate with tumor microvascular density [39], and it is suggested that blood flow, blood volume and the PS product are elevated in tumors [38]. Figures 4c and d show the increased blood volume and PS product in a prostate tumor. The blood volume and PS maps were calculated using the same method as Roberts *et al.* [31].

Heart attack

At an incidence rate of 20%, ischemic heart disease accounts for the highest percentage of deaths among North Americans. Accurate diagnosis, selection of treatment options, and follow-up of treatments require quantitative measurement of myocardial blood flow. As the heart is continuously beating, functional CT scanning has to be combined with retrospective electrocardiogram (ECG) gating. Serial CT scans of the heart are reconstructed every 100 ms from projection data collected within a window of 320 ms. By correlating the acquisition time of the serial scans with the ECG signal retrospectively, the end-diastolic scan of the heart can be selected for each heart beat. Blood flow maps (e.g. Figs 4e,f) throughout the myocardium can then be calculated using the same method as Roberts *et al.* [31].

Future development

Functional CT has proven to be very versatile in the study of hemodynamics-related functions in the human body. Its application has expanded to include tissues and organs where there is leakage of contrast from the blood stream into the extravascular space. However, there remain several technical issues that could further improve the performance of functional CT once implemented. These include: (i) post-processing methods as suggested by Joseph *et al.* [41] to correct for beam hardening in myocardial blood flow studies; (ii) prospective rather than retrospective cardiac gating in myocardial blood flow studies to reduce radiation dose to the patient; and (iii) respiratory gating to improve functional studies of the lung. Finally, current axial coverage of CT scanners has limited functional CT to studies of function within a 2 cm slab of the tissue; future true volumetric CT scanners will permit volumetric functional studies to be performed.

Concluding remarks

Functional CT, like functional magnetic resonance imaging, is a convenient way to study physiological function in the human body. One of the main issues in functional CT is the selection of an appropriate tracer kinetics model to describe the distribution of contrast agent in tissue. To be realistic, this description must include: (i) the convective transport of the contrast agent owing to blood flow through the vasculature; (ii) the exchange of contrast agent between the blood stream and the extravascular space during the transit through the vasculature; (iii) the venous outflow of contrast agent that is not extracted; and (iv) the backflux of contrast agent from the extravascular to intravascular space. The Johnson and Wilson model [7] is the model of choice as it captures all of these essential features, whereas other models do not. Furthermore, with the adiabatic approximation proposed by St Lawrence and Lee [28], the model solution can be computed efficiently to enable the generation of functional maps of blood flow, blood volume, mean transit time and PS product from a single contrast-enhanced dynamic CT study.

Acknowledgements

This work is supported by the Canadian Institutes of Health Research and Ontario Research and Development Challenge Fund.

References

1 Ladurner, G. *et al.* (1976) Measurement of regional cerebral blood volume by computerized axial tomography. *J. Neurol. Neurosurg. Psychiatry* 39, 152–155

2 Traupe, H. *et al.* (1979) Hyperperfusion and enhancement in dynamic computed tomography of ischemic stroke patients. *J. Comput. Assist. Tomogr.* 3, 627–632

3 Kalender, W.A. (2000) *Computed Tomography*, Publicis MCD Verlag

4 Brooks, R.A. (1977) A quantitative theory of the Hounsfield unit and its application to dual energy scanning. *J. Comput. Assist. Tomogr.* 1, 487–493

5 Lassen, N.A. and Perl, W. (1977) *Tracer Kinetic Methods in Medical Physiology*, Raven Press

6 Patlak, C.S. *et al.* (1983) Graphical evaluation of blood-to-brain transfer constants from multiple-time uptake data. *J. Cereb. Blood Flow Metab.* 3, 1–7

7 Johnson, J.A. and Wilson, T.A. (1966) A model for capillary exchange. *Am. J. Physiol.* 210, 1299–1303

8 Peters, A.M. *et al.* (1987) Non-invasive measurements of blood flow and extraction fraction. *Nucl. Med. Commun.* 8, 823–837

9 Miles, K.A. (1991) Measurement of tissue perfusion by dynamic computed tomography. *Br. J. Radiol.* 64, 409–412

10 Klotz, E. and Konig, M. (1999) Perfusion measurements of the brain: using dynamic CT for the quantitative assessment of cerebral ischemia in acute stroke. *Eur. J. Radiol.* 30, 170–184

11 Cenic, A. *et al.* (1999) Dynamic CT measurement of cerebral blood flow: a validation study. *AJNR Am. J. Neuroradiol.* 20, 63–73

12 Jaschke, W.R. *et al.* (1987) Cine-CT measurement of cortical renal blood flow. *J. Comput. Assist. Tomogr.* 11, 779–784

13 Axel, L. (1980) Cerebral blood flow determination by rapid sequence computed tomography. *Radiology* 137, 679–686

14 Meier, P. and Zierler, K.L. (1954) On the theory of the indicator-dilution method for measurement of blood flow and volume. *J. Appl. Physiol.* 6, 731–744

15 Schumann, P. *et al.* (1998) Evaluation of the ratio of cerebral blood flow to cerebral blood volume as an index of local cerebral perfusion pressure. *Brain* 121, 1369–1379

16 Gobbel, G.T. *et al.* (1991) Measurement of regional cerebral blood flow using ultrafast computed tomography. Theoretical aspects. *Stroke* 22, 768–771

17 Bassingthwaighte, J.B. *et al.* (1970) Definitions and terminology for indicator dilution methods. In *Capillary Permeability* (Crone, C. and Lassen, N.A., eds), pp. 665–669, Munksgaard

18 Gamel, J. *et al.* (1973) Pitfalls in digital computation of the impulse response of vascular beds from indicator dilution curves. *Circ. Res.* 32, 516–523

19 Leggett, D.A.C. *et al.* (1999) Blood–brain-barrier and blood volume imaging of cerebral glioma using functional CT: a pictorial review. *Eur. J. Radiol.* 30, 185–190

20 Tsushima, Y. (1999) Functional CT of the kidney. *Eur. J. Radiol*. 30, 191–197

21 Groothuis, D.R. *et al.* (1991) Quantitative measurements of capillary transport in human brain tumors by computed tomography. *Ann. Neurol.* 30, 581–588

22 Yeung, I.W.T. *et al.* (1992) *In vivo* CT measurement of blood-brain transfer constant of iopamidol in human brain tumors. *J. NeuroOncology* 14, 177–187

23 Terada, T. *et al.* (1992) A method for quantitative measurement of cerebral vascular permeability using X-ray CT and iodinated contrast medium. *Neuroradiology* 34, 290–296

24 Bartolini, A. *et al.* (1993) Functional vascular volume and blood–brain barrier permeability images by angio-CT in the diagnosis of cerebral lesions. *Comput. Med. Imaging Graph.* 17, 35–44

25 Martene, R. *et al.* (2000) Non-invasive quantification of liver perfusion with dynamic computed tomography and a dual-input one-compartment model. *Clin. Sci.* 99, 517–525

26 Rapoport, S. (1976) *Blood–Brain Barrier in Physiology and Medicine*, Raven Press

27 Crone, C. (1963) The permeability of capillaries in various organs as determined by use of the 'indicator diffusion' method. *Acta Physiol. Scand.* 58, 292–305

28 St Lawrence, K.S. and Lee, T.Y. (1998) An adiabatic approximation to the tissue homogeneity model for water exchange in the brain I. Theoretical derivation. *J. Cereb. Blood Flow Metab.* 18, 1365–1377

29 St Lawrence, K.S. and Lee, T.Y. (1998) An adiabatic approximation to the tissue homogeneity model for water exchange in the brain II. Experimental validation. *J. Cereb. Blood Flow Metab.* 18, 1378–1385

30 Purdie, T.G. *et al.* (2001) Functional CT imaging of angiogenesis in rabbit VX2 soft-tissue tumor. *Phys. Med. Biol.* 46, 3161–3175

31 Roberts, H.C. *et al.* (2002) Dynamic, contrast-enhanced CT of human brain tumors: quantitative assessment of blood volume, blood flow, and microvascular permeability: report of two cases. *AJNR Am. J. Neuroradiol.* 23, 828–832

32 Nabavi, D.G. *et al.* (2001) Perfusion mapping using computed tomography allows accurate prediction of cerebral infarction in experimental brain ischemia. *Stroke* 32, 175–183

33 Koenig, M. *et al.* (2001) Quantitative assessment of the ischemic brain by means of perfusion-related parameters derived from perfusion CT. *Stroke* 32, 431–437

34 Eastwood, J.D. *et al.* (2002) CT perfusion scanning with deconvolution analysis: pilot study in patients with acute middle cerebral artery stroke. *Radiology* 222, 227–236

35 Wintermark, M. *et al.* (2002) Prognostic accuracy of cerebral blood flow measurement by perfusion computed tomography, at the time of emergency room admission, in acute stroke patients. *Ann. Neurol.* 51, 417–432

36 Hamberg, L.M. *et al.* (1996) Measurement of cerebral blood volume with subtraction three-dimensional functional CT. *AJNR Am. J. Neuroradiol.* 17, 1861–1869

37 Lev, M.H. *et al.* (2001) Utility of perfusion-weighted CT imaging in acute middle cerebral artery stroke treated with intra-arterial thrombolysis: prediction of final infarct volume and clinical outcome. *Stroke* 32, 2021–2028

38 Miles, K.A. *et al.* (2000) Application of CT in the investigation of angiogenesis in oncology. *Acad. Radiol.* 7, 840–850

39 Swensen, S.J. *et al.* (1996) Lung nodule enhancement at CT: prospective findings. *Radiology* 201, 447–455

40 Rumberger, J.A. *et al.* (1987) Use of ultrafast computed tomography to quantitate regional myocardial perfusion: a preliminary report. *J. Am. Coll. Cardiol.* 9, 59–69

41 Joseph, P.M. and Ruth, C. (1997) A method for simultaneous correction of spectrum hardening artifacts in CT images containing both bone and iodine. *Med. Phys.* 24, 1629–1634